Hindawi
Mathematical Problems in Engineering
Volume 2021, Article ID 8270793, 8 pages
https://doi.org/10.1155/2021/8270793

Research Article

Restriction of Transverse Feedback Linearization for Piecewise Linear Paths

Gildeberto de Souza Cardoso,[1] **Leizer Schnitman**,[2] **José Valentim dos Santos Filho**,[1] **and Luiz Carlos Simões Soares Júnior**[1]

[1]*Universidade Federal do Recôncavo da Bahia, R. Rui Barbosa 710-Centro, Cruz das Almas, BA, Brazil*
[2]*Universidade Federal da Bahia, R. Prof. Aristides Novis 2-Federação, Salvador, BA, Brazil*

Correspondence should be addressed to Gildeberto de Souza Cardoso; gildeberto@ufrb.edu.br

Received 3 August 2020; Revised 8 January 2021; Accepted 13 January 2021; Published 30 January 2021

Academic Editor: Jerzy Baranowski

Copyright © 2021 Gildeberto De Souza Cardoso et al. This is an open access article distributed under the Creative Commons Attribution License, which permits unrestricted use, distribution, and reproduction in any medium, provided the original work is properly cited.

This work presents a path-following controller for a unicycle robot. The main contribution of this paper is to demonstrate the restriction of transverse feedback linearization (TFL) to obtuse angles on piecewise linear paths. This restriction is experimentally demonstrated on a Kobuki mobile robot, where it is possible to observe, as a result of the limitation of the TFL, the convergence to another domain of attraction.

1. Introduction

Mobile robot applications have significantly increased in recent years. Following a general rule of technological evolution, mobile robotics has increasingly prioritized autonomy in relation to the environment, requiring greater efficiency of navigation and control systems. To ensure that a robot follows a reference path or to stabilize a robot at a desired point, a motion control system is needed. According to the type of reference to be followed by the mobile robot, the motion control systems are classified into three types:

(1) Point stabilization
(2) Trajectory tracking
(3) Path following

The objective of point stabilization is to stabilize the robot in a certain desired position. According to [1], this objective cannot be achieved with continuous or smooth state feedback control laws if the robot is subject to nonholonomic constraints. In this case, approaches such as control laws that vary slightly in time [2] and discontinuous and hybrid feedbacks [3] can be used. Another way to avoid the problem of nonholonomy is the use of Frenet–Serret and Triedro [4] to describe the state space.

In trajectory tracking, the control laws that act on the robot must follow a parameterized law of timing associated with the movement.

In path following, the robot converges and follows a predefined path. This path does not have any temporal specification. The robot tracks a desired speed profile, and the controller acts on the orientation to drive the robot along the intended path [5].

Of the three categories described above, we chose the path-following technique for this work. In the path-following control, the forward speed of the robot tracks the desired speed profile, while the controller acts on the orientation of the robot in order to steer the vehicle along the path. Usually, smoother convergence to a path is achieved when path-following strategies are used compared with trajectory-tracking control laws [6].

There are several cases in which a path-following controller is appropriate for nonholonomic robotic systems, such as Samson [7], Morro et al. [8], Pazderski [9], and Soetanto et al. [10].

Approach for path following is transverse feedback linearization (TFL). The main advantage of adopting TFL is that the controllers guarantee path invariance. Some path-following control techniques, such as sliding control, do not have this property. Path invariance means that if the robot starts with tangential velocity to the path, the robot will remain on the path for all future time [11].

There are many examples in the literature of the use of TFL to control robotics systems.

In Nielsen and Maggiore [12], the authors solve the TFL for a car-like robot with fixed translational velocity. Akhtar and Nielsen [13] propose a path-following controller for a kinematic model of car-like mobile robots using TFL and tangential dynamic extension. Akhtar et al. [14] propose a path-following controller for a quadrotor using TFL and tangential dynamic extension. In Hladio et al. [15], the authors propose a path-following controller for a five-bar robotic manipulator using TFL to put the system into a normal form for control design. Akhtar et al. [11] propose path-following controllers for the kinematic model of car-like mobile robots using TFL with dynamic extension. Dovgobrod [16] proposes an algorithm to provide a precision stabilization of a vehicle on a path. Finally, Nguyen et al. [17] design a controller combining model predictive control and TFL techniques.

This article analyzes the response of TFL in relation to the piecewise linear path and, as its main contribution, demonstrates analytically the restriction to an obtuse path. This limitation is experimentally verified on a Kobuki mobile robot.

2. Problem Formulation

In this section, we demonstrate path-following controllers for a kinematic model of a unicycle. The following properties of the path-following strategy are assumed:

(1) The robot is able to plan a piecewise linear path from the starting position to the goal position

(2) Each line segment of the path should be controlled invariant

2.1. Kinematic Model of Robot. Consider the kinematic model of a unicycle mobile robot shown in Figure 1:

$$\begin{aligned} \dot{x}_1(t) &= v(t)\cos\left(x_3(t)\right), \\ \dot{x}_2(t) &= v(t)\sin\left(x_3(t)\right), \\ \dot{x}_3(t) &= \omega(t). \end{aligned} \tag{1}$$

Here, $(x_1, x_2) \in \mathbb{R}^2$ represents the robot's position in the plane, and $x_3 \in \mathbb{S}$ is the robot's heading. The control inputs are the translational speed $v \in \mathbb{R}$ and the angular velocity $\omega \in \mathbb{S}$. The output of the system is the robot's location in the plane, which is given by

$$y(t) = Cx(t) = \begin{bmatrix} 1 & 0 & 0 \\ 0 & 1 & 0 \end{bmatrix} x(t). \tag{2}$$

The configuration space of (1) is $\mathcal{X} = \mathbb{R}^2 \times \mathbb{S}$, and the output space of (2) is $\mathcal{Y} = \mathbb{R}^2$. It is assumed that only the position coordinates of a robot are measured and continuous updates are provided in its state vector x. The heading vector is defined as $\tau(x_3) = (\sin(x_3), \cos(x_3))$; its Euclidean norm equals 1 and it points in the direction the robot is facing Figure 1.

2.2. Workspace. The unicycle robot model (1) operates in a workspace $W \subset \mathbb{R}^2$. The set W is assumed to be compact and path-connected with a nonempty interior. The output space has a finite number of obstacles $O_i \subset \mathbb{R}^2$, $i \in \{1, \ldots, n\}$. Each obstacle O_i is assumed to be a closed, convex set. The free workspace is defined as $W_{\text{free}} = W \setminus (O_1 \cup O_2 \cup \cdots \cup O_n)$.

The differential drive robot moves in the environment under the assumption that models (1) and (2) have a map of W_{free} stored in its memory, which contains two distinguished points $p_{\text{start}}, p_{\text{goal}} \in W_{\text{free}}$.

2.3. Configuration Map. In order to model the fact that the robot is not simply a point with no area in its workspace, this section introduces the notion of a map.

Definition 1. There exists a set-valued function $B: \rightrightarrows$ called the configuration map that maps each configuration $x \in \mathcal{X}$ of robot (1) to the set of all points $B(x) \subset \mathcal{Y}$ belonging to the robot.

As depicted in Figure 1, it is assumed that the differential drive robot has a polygonal shape. Therefore, $B(x)$ is a polygonal region in the plane, for $B(x(t)) \subset W_{\text{free}}$ is necessary to ensure that there are no collisions, during the period of time in which the robot is moving from the start to the goal position.

2.4. Path-Following Outputs for Path Planners. The path-following output associated to a smooth parameterized curve $\sigma: \mathbb{R} \longrightarrow \mathbb{R}^p$ was defined in [18]. It consists of two complementary objects: a transversal output and a tangential output. The transversal output is a smooth function $\mu: U \subseteq \mathbb{R}^p \longrightarrow \mathbb{R}^{p-1}$ with the property that zero is a regular value of the function and $\mu^{-1}(0) = \sigma(\mathbb{R})$. The tangential output is a projection $\varpi: U \subseteq \mathbb{R}^p \longrightarrow \mathbb{R}$ which, given an output location $y \in U$, returns the value of $\lambda \in \mathbb{R}$ with the property that $\sigma(\lambda)$ is the closest point to y on the given curve.

The resulting function $h_{\text{PF}}: U \subseteq \mathbb{R}^p \longrightarrow \mathbb{R}^p$, and $y \mapsto (\varpi(y), \mu(y))$ is the path-following output. This virtual output has a clear physical meaning for path-following control design and can be viewed as a local diffeomorphism on the output space of the robot. In this section, keeping in mind that the paths will be generated as a sequence of waypoints, a procedure is presented to generate a set of linear path-following outputs from a sequence of waypoints.

Suppose that a sample-based path planner has returned a path from p_{start} to p_{goal} as a sequence of points in W_{free}

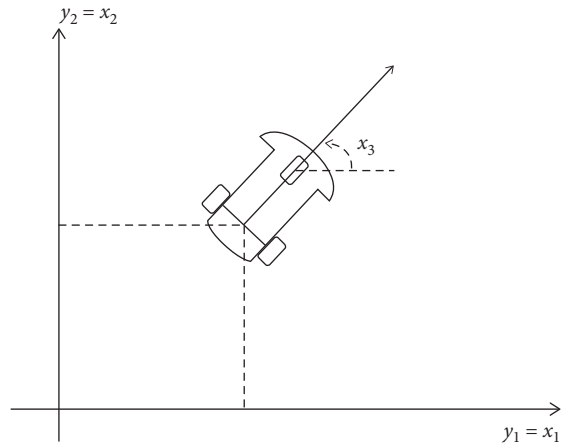

Figure 1: Unicycle robot.

which is a subset of a p-dimensional real vector space $\mathcal{Y}$ (because the results of this section apply equally well in higher dimensions, we do not assume that the workspace of our robot is a subset of $\mathbb{R}^2$ as in the case of the differential drive robot). That is, given a set $\{p_1, p_2, \ldots, p_{N-1}, p_N\}$ with $p_1 = p_{\text{start}}$, $p_N = p_{\text{goal}}$ and each $p_i \in \mathcal{Y}$. To avoid trivial cases, assume that, for each $i \in \mathbb{N}_{N-1}$, $p_i \neq p_{i+1}$. These points represent a planned path consisting of $N-1$ line segments $\ell_i = \overline{p_i p_{i+1}} \subset \mathcal{Y}$, $i \in \mathbb{N}_{N-1}$ of nonzero length. A path-following output h^i_{PF} is associated with each line segment ℓ_i.

The span of the vector $p_{i+1} - p_i \in \mathcal{Y}$ is a 1-dimensional subspace that is parallel to the (infinite) line passing through the line segment ℓ_i. The $(p-1)$-dimensional subspace $\mathcal{V}_i = \text{Ker}(p_{i+1}^\top - p_i^\top)$ consists of vectors which annihilate $(p_{i+1} - p_i)^\top$. Let V_i: $\mathcal{V}_i \longrightarrow \mathcal{Y}$ be the insertion map. The insertion map is represented by any matrix whose column vectors form a basis for $\mathcal{V}_i$ relative to the given basis for $\mathcal{Y}$. Finally, denote its associated dual map by $V_i^\top$: $\mathcal{V}' \longrightarrow \mathcal{V}_i'$. By construction, it is determined that $V_i^\top (p_{i+1} - p_i) = 0$. A zero-level set representation of the affine subspace containing ℓ_i is obtained using

$$d_i = -V_i^\top p_i, \tag{3}$$

where $d_i \in \mathbb{R}$

It is now claimed that $\ell_i \subset \{y \in \mathcal{Y}: V_i^\top y + d_i = 0\}$. If $y \in \ell_i$, then it can be expressed as a convex combination of p_i and p_{i+1}, i.e., $y = \lambda p_i + (1-\lambda) p_{i+1}$, $\lambda \in [0,1]$. Therefore,

$$\begin{aligned} V_i^\top y + d_i &= \lambda V_i^\top (p_i - p_{i+1}) + V_i^\top p_{i+1} + d_i \\ &= V_i^\top p_{i+1} + d_i \\ &= V_i^\top (p_{i+1} - p_i) \\ &= 0. \end{aligned} \tag{4}$$

The set

$$\mu_i(y) = V_i^\top y + d_i, \tag{5}$$

and so the value of the transversal part of the path-following output associated to the line segment ℓ_i has been calculated. Repeating this for each line segment, a set of pairs $\mathcal{S} = \{(V_1^\top, d_1), \ldots, (V_{N-1}^\top, d_{N-1})\}$ is generated from the set of waypoints.

To compute the tangential part of the path-following output associated to ℓ_i, a constrained optimization problem is solved. To begin, a parametrization of ℓ_i is generated. Next, l_i and m_i are defined: $l_i = \|p_i - p_{i+1}\|_2$ and $m_i = (p_i - p_{i+1})/l_i$. Then, the curve σ_i is defined as $[0, l_i] \longrightarrow \mathcal{Y}$ via $\sigma_i(\lambda) = m_i \lambda + p_i$. It follows that $\sigma_i([0, l_i]) = \ell_i$. Given a point $y \in \mathcal{Y}$, consider the constrained optimization problem.

Problem 1

$$\begin{aligned} &\underset{y^*}{\text{minimize}}: \ \|y - y^*\|_2, \\ &\text{subject to}: \quad V_i^\top y^* + d_i = 0. \end{aligned} \tag{6}$$

Using Lagrange multipliers, the minimizing argument is given by

$$y^* = \left(I - V_i (V_i^\top V_i)^{-1} V_i^\top\right) y + (V_i^\top V_i)^{-1} d_i. \tag{7}$$

The value of $\lambda^* \in [0, l_i]$ for which $\sigma_i(\lambda^*) = y^*$ can now be computed yielding the second part of the path-following output for line segment ℓ_i:

$$\varpi_i(y) = m_i^\top (y^* - p_i). \tag{8}$$

In summary, equations (5)–(8) define the path-following output $h^i_{\text{PF}}(y) = (\mu_i(y), \varpi_i(y))$ associated to each line segment $\ell_i = \overline{p_i p_{i+1}}$. This output happens to be a linear affine function of y:

$$h^i_{\text{PF}}(y) = \begin{bmatrix} m_i^\top \\ V_i^\top \end{bmatrix} y + \begin{bmatrix} m_i^\top \left((V_i^\top V_i)^{-1} d_i - p_i \right) \\ d_i \end{bmatrix}. \tag{9}$$

Using the fact that $m_i^\top V_i = 0$ to simplify notation, let $n_i = m_i^\top (V_i^\top V_i)^{-1} d_i - m_i^\top p_i$; then, (9) can be written:

$$h^i_{\text{PF}}(y) = \begin{bmatrix} m_i^\top \\ V_i^\top \end{bmatrix} y + \begin{bmatrix} n_i \\ d_i \end{bmatrix}. \tag{10}$$

The set is further defined as follows:

$$\mathcal{T} = \{(m_1^\top, n_1), \ldots, (m_{N-1}^\top, n_{N-1})\}, \tag{11}$$

and then, each line segment ℓ_i is associated with the pairs

$$\begin{aligned} &(V_i^\top, d_i) \in \mathcal{S}, \\ &(m_i^\top, n_i) \in \mathcal{T}. \end{aligned} \tag{12}$$

3. Transverse Feedback Linearization

Consider the differential drive robot configurations (1) and (2). Assume that the robot's translational speed v is a fixed positive constant. In addition, as in Section 2, a sample-based path planner has returned a path from p_{start} to p_{goal} as a sequence of points $\{p_1, p_2, \ldots, p_{N-1}, p_N\}$ in $W_{\text{free}} \subset \mathbb{R}^2$. Following the construction of Section 2.4, the sets $\mathcal{S}$ and $\mathcal{T}$ are known. Then, for each $i \in \mathbb{N}_{N-1}$, the robot's path-following output is given by

$$y_{\text{PF}}^i := h_{\text{PF}}^i(Cx) = \begin{bmatrix} m_i^\top C \\ V_i^\top C \end{bmatrix} x + \begin{bmatrix} n_i \\ d_i \end{bmatrix}. \tag{13}$$

The path-following manifold of ℓ_i is the largest controlled invariant set containing the lift of the path

$$\Gamma^i = \{x \in \mathcal{X} \colon V_i^\top C x + d_i = 0\}. \tag{14}$$

It is verified that y belongs to the line that contains ℓ_i if and only if $x \in \Gamma^i$. Of course, Γ^i is not controlled invariant: if the robot is initialized on ℓ_i but with $\tau(x_3(0))$ parallel Γ^i to V_i, then the robot must leave the set before possibly returning to the set. From a planning point of view, such behaviors are obviously undesirable because they could lead to large deviations from the planned path and therefore collisions.

The direction in which the robot travels along the line depends on its initial conditions, which determine which component Γ_*^i ($\Gamma_{(*,+)}^i$ or $\Gamma_{(*,-)}^i$) the robot approaches. In the path-planning framework, the robot must move in a prescribed direction along each segment ℓ_i. This ensures that the robot always approaches $\Gamma_{(*,+)}^i$ so that it moves in the correct direction.

The path-following manifold of the line $\sigma_i(\lambda) = n_i\lambda + p_i$, $\lambda \in \mathbb{R}$, with respect to the differential drive robot (1) and (2) is given by a union of disjoint closed sets:

$$\Gamma_*^i = \Gamma_{(*,+)}^i \cup \Gamma_{(*,-)}^i, \tag{15}$$

where

$$\Gamma_{(*,+)}^i = \left\{x \in \Gamma^i \colon V_i^\top \tau(x_3), x_3 = \arg(v_2 - jv_1)\right\}, \tag{16}$$

$$\Gamma_{(*,-)}^i = \left\{x \in \Gamma^i \colon V_i^\top \tau(x_3), x_3 = \arg(-v_2 + jv_1)\right\}, \tag{17}$$

and $V_i^\top = \begin{bmatrix} v_1 & v_2 \end{bmatrix}$. Furthermore, $\operatorname{dist}(\Gamma_{(*,+)}^i, \Gamma_{(*,-)}^i) = \pi$, where $\operatorname{dist}(A, B) = \inf\{\|a - b\| \mid a \in A, b \in B\}$.

Sets (16) and (17) are disjoint because $x_3 \in \mathcal{S}$, and set (15) is closed because its complement is open. The complement is given by $\Gamma^c = \mathbb{R}^p \backslash \Gamma = \{y \in \mathbb{R}^p \colon V_i^\top C x + d_i \neq 0\}$ and the empty set is open by definition.

Γ_* is the controlled invariant set. Physically, it consists of all motions of the unicycle robot (1) for which the output signal (2) can be made to remain on the curve σ_i.

To prove, it is necessary to show that $V_i^\top C x + d_i$ has a well-defined relative degree.

Proof. Let

$$\xi_k^i = \begin{bmatrix} \xi_1^i \\ \xi_2^i \end{bmatrix} = \begin{bmatrix} V_i^\top C x + d_i \\ V_i^\top \tau(x_3) \end{bmatrix}. \tag{18}$$

Recall $v(t) \neq 0$; the denominator of control (20) goes to zero if and only if $x_3 = \arctan(x_2/x_1)$. However, this condition is not allowed on Γ_*. Suppose, by contradiction, that this occurs. Then, because $\xi_1 = \xi_2 = 0$,

$$\begin{bmatrix} \cos x_3 & \sin x_3 \\ -\sin x_3 & \cos x_3 \end{bmatrix} \begin{bmatrix} x_1 \\ x_2 \end{bmatrix} = 0, \tag{19}$$

is nonsingular. Because $V_i^\top C x + d_i = 0$, it is not possible for $x_1 = x_2 = 0$. The function ξ_k yields a well-defined relative degree $n^* = 2$, where $n^* = \dim(\Gamma_*)$. □

If the input $u := \omega$, the feedback controller can be expressed mathematically as follows:

$$u = \frac{-k_i^\top \xi_k^i}{V_i^\top R_{\pi/2} \tau(x_3)}, \tag{20}$$

where $R_{\pi/2} = \begin{bmatrix} 0 & -1 \\ 1 & 0 \end{bmatrix}$ and $k_i \in \mathbb{R}_{\geq 0}^2$.

Controller (20) is well defined on the open set $\mathcal{X} \backslash \{x \in \mathcal{X} \colon \arg(e^{j(x_3 - x_3^+)}) = (\pi/2)\}$, the feedback controller will result in a closed-loop system whose trajectories approach Γ_*^i, and therefore, the output y will approach the line $\sigma(\lambda)$.

4. Supervisory Control of TFL Path-Following Controllers

As shown in Section 3, on each line segment ℓ_i, controller (20) drives the robot to its path-following manifold. This section describes how the robot is switched from one line segment to the next and also how the convergence to $\Gamma_{(*,+)}^i$ is ensured.

Let $\eta_1^i = m_1^\top C x + n_i$. This tangential state describes the robot's position on ℓ_i. When $\eta_i = 0$, the closest point to the robot's output on the path defined by $\{p_1, \ldots, p_{N-1}\}$ is p_i. When $\eta_1^i = l_i$, the closest point is p_{i+1}. With this in mind, the algorithmic state machine shown in Figure 2 is used to supervise our path-following controllers.

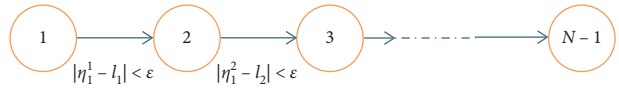

Figure 2: State diagram of the supervisory controller.

In state i, the robot's control signal is given (10) by $(V_i^\top, d_i) \in \mathcal{S}$ and $(m_i^\top, n_i) \in \mathcal{T}$. The supervisory control monitors how far the robot is from the next waypoint. When that distance is sufficiently small, controller (20) changes its parameters to $(V_{i+1}^\top, d_{i+1}) \in \mathcal{S}$, $(m_{i+1}^\top, n_i) \in \mathcal{T}$.

In principle, controller (20) can use a different set of gains $k_i \in \mathbb{R}^2_{\geq 0}$ on each line segment. However, as the next proposition shows, a single set of gain values is chosen to ensure that the robot transitions from $\Gamma^i_{(*,+)}$ to $\Gamma^{i+1}_{(*,+)}$ and thus moves in the correct direction along the paths.

Proposition 1. *With respect to system (18), a set $\mathcal{U}_i^+$ is defined by*

$$\mathcal{U}_i^+ = \left\{ x \in \mathcal{X} : \left| \arg\left(e^{j(x_3 - x_3^+)} \right) \right| < \frac{\pi}{2} \right\}, \tag{21}$$

where $x_3^+ = arg(v_2 - jv_1)$ is positively invariant if controller (20) is used with

$$k_i^\top = [\, k_1 \;\; k_2 \,], \quad \text{with } k_2 > \sqrt{4k_1}. \tag{22}$$

Proof. The Laplace transform is used to prove the existence of a domain of attraction for the system under analysis. Those domains of attraction, shown in Figure 3, are defined for Γ_* as

$$\begin{aligned} \mathcal{U}_i^+ &= \left\{ x \in \mathcal{X} : \left| \arg\left(e^{j(x_3 - x_3^+)} \right) \right| < \frac{\pi}{2} \right\}, \\ \mathcal{U}_i^- &= \left\{ x \in \mathcal{X} : \left| \arg\left(e^{j(x_3 - x_3^-)} \right) \right| < \frac{\pi}{2} \right\}. \end{aligned} \tag{23}$$

It can be stated that path following is an output zeroing problem. Therefore, it is necessary to show that $\xi_2(t) \leq \xi_2(0), \forall t \geq 0$.

ξ_2 can be described as follows:

$$\xi_2 = \|V_i^\top\| \|\tau(x)\| \cos\phi. \tag{24}$$

If $\|V_i^\top\|$ is normalized so that it is equal to 1, $\|\tau(x)\| = 1$; therefore, it can be deduced that $\xi_2 = 0$ if and only if $\phi = \pm(\pi/2)$. If $\phi = k\pi$ for $k \in \mathbb{N}$. There is a singularity because, in this case, $\xi_2 = \pm 1$.

For this case, it is sufficient to prove that $\xi_2(t) \leq \xi_2(0)$, see Figure 4

$$\dot{\xi}_1 = \xi_2, \tag{25}$$

$$\dot{\xi}_2 = -k_1\xi_1 - k_2\xi_2. \tag{26}$$

From expression (25),

$$\ddot{\xi}_2 + k_2\dot{\xi}_2 + k_1 \int_0^t \xi_2(\tau)\mathrm{d}\tau = 0. \tag{27}$$

Developing the above differential equation using the Laplace transform yields the following:

$$\begin{aligned} s\widehat{\xi}_2 - \xi_2(0) + k_2\widehat{\xi}_2 &= -\frac{k_1}{s}\widehat{\xi}_2, \\ \mathcal{L}\{\xi_2\} &= \widehat{\xi}_2, \\ \left(s + k_2 + \frac{k_1}{s} \right)\widehat{\xi}_2 &= \xi_2(0), \\ \widehat{\xi}_2 \left(\frac{s^2 + k_2 s + k_1}{s} \right), &= \xi_2(0), \\ \widehat{\xi}_2 &= \frac{s\xi_2(0)}{s^2 + k_2 s + k_1}, \\ \frac{\widehat{\xi}_2}{\xi_2(0)} &= \frac{s}{s^2 + k_2 s + k_1} = \frac{sk\omega_n^2}{s^2 + 2\varepsilon\omega_n s + \omega_n^2}. \end{aligned} \tag{28}$$

Therefore, if $\omega_n^2 = k_1$, $\varepsilon = (k_2/2\sqrt{k_1})$ and $k = (1/\omega_n^2)$; if $\varepsilon > 1$, there exist two real poles:

$$\begin{aligned} G(s) &= \frac{skab}{(s+a)(s+b)}, \\ \xi_2(t) &= \frac{\mathrm{d}}{\mathrm{d}t}\left(\left(\frac{kab}{b-a}\left(e^{-at} - e^{-bt} \right)\xi_2(0) \right) \right), \\ \xi_2(t) &= \frac{kab}{b-a}\left(-ae^{-at} + be^{-bt} \right)\xi_2(0). \end{aligned} \tag{29}$$

Recall $k = (1/k_1) = (1/ab)$:

$$\xi_2(t) = \frac{1}{b-a}\left(-ae^{-at} + be^{-bt} \right)\xi_2(0). \tag{30}$$

Therefore, if $k_2 > \sqrt{4k_1}$, $|\xi_2(0)| > |\xi_2(t)|$ and U^+ is positively invariant, $\xi_2(t, \xi_0) \in U^+, \forall t \geq 0$.

Because the transversal proportional controller is given by

$$v^{\pitchfork}(\xi) = -k^\top \xi^i, \tag{31}$$

$v^{\pitchfork}(0)$, $\xi = 0$ is an equilibrium point of the closed-loop transversal system. As a consequence, path invariance is achieved, meaning that if the robot is initialized in the path, it will remain in the path at all future points. □

Thus, any initial condition in $\mathcal{U}_i^+$ results in trajectories that approach $\Gamma^i_{(*,+)}$, assuming the gains in (20) are chosen properly.

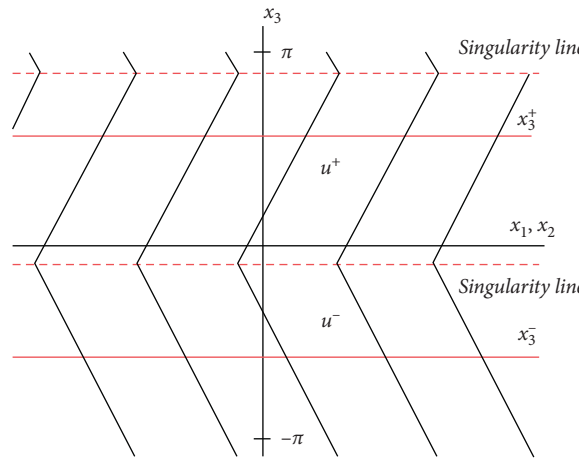

Figure 3: Domains of attraction.

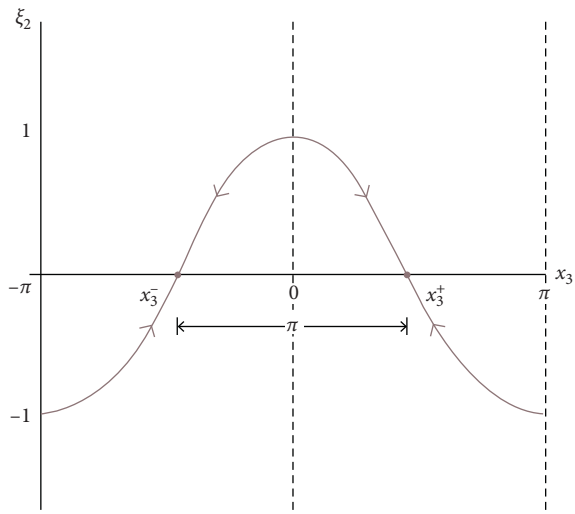

Figure 4: ξ_2 vs.x_3.

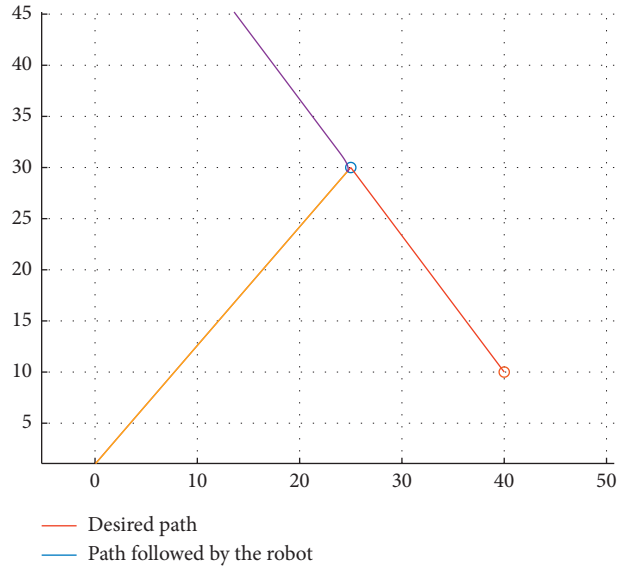

Figure 5: TFL response to the obtuse angle path.

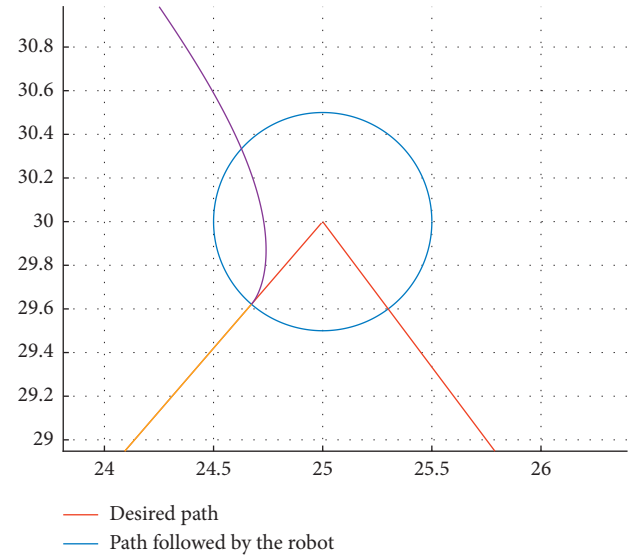

Figure 6: TFL response to the obtuse angle path.

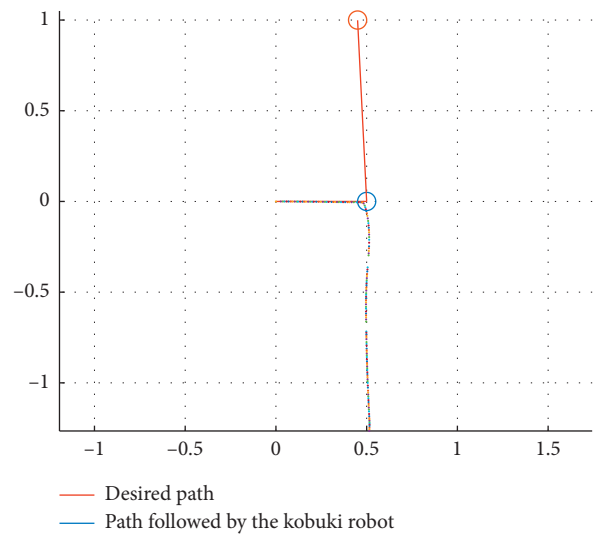

Figure 7: Experimental TFL response to the obtuse angle path.

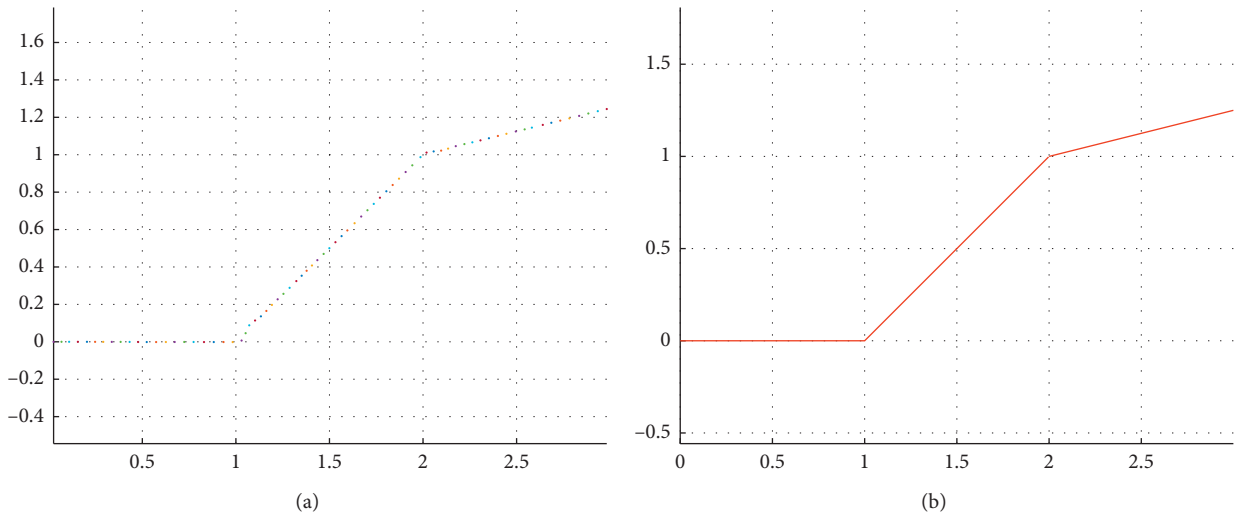

Figure 8: Experimental TFL response to the acute angle path. (a) Kobuki mobile robot following piecewise linear path. (b) Desired path.

As a result when the supervisory control switches at time, from state i to state $i+1$, the controller will cause the robot to traverse the path in the desired direction so long as

$$x(T) \in \mathcal{U}_i^+ \cap \mathcal{U}_{i+1}^+. \tag{32}$$

Because controller (20) exponentially stabilizes Γ_*^i, it is reasonable to assume that $x(T) \in \Gamma_{(*,+)}^i$ or is very close to it. As such, the next result says that if the robot is traversing segment ℓ_i in the correct direction, it will continue to traverse ℓ_{i+1} in the desired direction if $\Gamma_{(*,+)}^i \cap \mathcal{U}_{i+1}^+ \neq \varnothing$.

5. Results and Conclusion

In this section, simulation results dealing with the TFL and experiments on Kobuki mobile robot are presented. The limitation of the TFL is illustrated by showing the robot's inability to follow paths with obtuse angles.

In order to demonstrate the robot's inability to correctly follow a path with obtuse angles, a control was implemented to follow the points [0 1; 25 30; 40 10] whose distance between them is Euclidean. The angle between the yellow and red straight segments is 102.37°, and the robot's initial state was $x_0 = (0, 1, (\pi/4))$. As a result, a convergence to another attraction domain was observed; consequently, the robot followed the opposite trajectory, as shown in Figure 5. In this figure, the red straight segment indicates the desired path and the purple straight segment indicates the path followed by the robot.

Circles were drawn at each point. The radius of these circles, $\varepsilon = 0.5$, defines the path switching area; if the robot gets close enough as to the target point, the controller can then guide the robot through the next path. Such a transition can be observed in Figure 6.

Tests were performed on a robotic platform called Kobuki, made by Yujin Robot. It is controlled by an embedded Raspberry Pi 3 microcontroller running ROS (Robotic Operational System). Matlab software on a second computer was used to run the TFL controller, which communicated with the robot through an IEEE 802.11 wireless network.

The Kobuki mobile robot was asked to follow a set of points whose distance is Euclidean between them. To demonstrate the robot's inability to follow an obtuse path, points $[(0,0), (0.5,0), (0.45,1)]$ were selected as the robot's path, with the initial position given by $x_0 = (0,0,0)$ and the gains given by $k_1 = 2$ and $k_2 = 2.84$. As expected, the robot followed another attraction domain, as shown in Figure 7.

On the contrary, when the trajectory has only acute angles, the robot remains on the path. Figure 8(a) shows that the robot remains on the desired path Figure 8(b) and follows it. The initial position is given by $x_0 = (0,0,0)$; the points followed by the robot were $(0,0)$, $(1,0)$, $(2,1)$, and $(3,1.25)$; the gains were given by $k_1 = 2$ and $k_2 = 2.84$.

In this paper, a path-following controller has been designed for a Kobuki mobile robot, using transverse feedback linearization for piecewise linear paths. The restriction of TFL was demonstrated using a kinematic model of a unicycle mobile robot. It has been shown that when the path has obtuse angles, the robot follows another domain of attraction, making the TFL unfeasible in these cases.

Data Availability

No data were used to support this study.

Conflicts of Interest

The authors declare that they have no conflicts of interest.

References

[1] R. W. Brockett, "Asymptotic stability and feedback stabilization," in *Differential Geometric Control Theory*, pp. 181–191, Birkhauser, Basel, Switzerland, 1983.

[2] L. Yiming, L. Ye, and W. Qi, "Design for three-dimensional stabilization control of underactuated autonomous underwater vehicles," *Ocean Engineering*, vol. 150, pp. 327–336, 2018.

[3] M. V. Dolgopolik and A. L. Fradkov, "Nonsmooth speed-gradient algorithms," in *Proceedings of the 2015 European Control Conference (ECC)*, Linz, Austria, July 2015.

[4] L. Lapierre, R. Zapata, and P. Lepinay, "Combined path-following and obstacle avoidance control of a wheeled robot," *The International Journal of Robotics Research*, vol. 26, no. 4, pp. 361–375, 2007.

[5] L. Adouane, *Autonomous Vehicle Navigation: From Behavioral to Hybrid Multi-Controller Architectures*, A. K. Peters, Ltd., Natick, MA, USA, 2016.

[6] L. Lapierre and D. Soetanto, "Nonlinear path-following control of an AUV," *Ocean Engineering*, vol. 34, no. 11-12, pp. 1734–1744, 2007.

[7] C. Samson, "Control of chained systems application to path following and time-varying point-stabilization of mobile robots," *IEEE Transactions on Automatic Control*, vol. 40, no. 1, pp. 64–77, 1995.

[8] A. Morro, A. Sgorbissa, and R. Zaccaria, "Path following for unicycle robots with an arbitrary path curvature," *IEEE Transactions on Robotics*, vol. 27, no. 5, pp. 1016–1023, 2011.

[9] D. Pazderski, "Waypoint following for differentially driven wheeled robots with limited velocity perturbations," *Journal of Intelligent & Robotic Systems*, vol. 85, no. 3-4, pp. 553–575, 2017.

[10] D. Soetanto, L. Lapierre, and A. Pascoal, "Adaptive, non-singular path-following control of dynamic wheeled robots," in *Proceedings of the 42nd IEEE International Conference on Decision and Control (IEEE Cat. No.03CH37475)*, vol. 2, pp. 1765–1770, Piscataway, NJ, USA, January 2003.

[11] A. Akhtar, C. Nielsen, and S. L. Waslander, "Path following using dynamic transverse feedback linearization for car-like robots," *IEEE Transactions on Robotics*, vol. 31, no. 2, pp. 269–279, 2015.

[12] C. Nielsen and M. Maggiore, "Maneuver regulation via transverse feedback linearization: theory and examples," in *Proceedings of the 6th IFAC Symposium on Nonlinear Control Systems 2004 (NOLCOS 2004)*, vol. 37, no. 13, pp. 57–64, Stuttgart, Germany, September 2004.

[13] A. Akhtar and C. Nielsen, "Path following for a car-like robot using transverse feedback linearization and tangential dynamic extension," in *Proceedings of the 2011 50th IEEE Conference on Decision and Control and European Control Conference*, pp. 7974–7979, Orlando, FL, USA, December 2011.

[14] A. Akhtar, S. L. Waslander, and C. Nielsen, "Path following for a quadrotor using dynamic extension and transverse feedback linearization," in *Proceedings of the 2012 IEEE 51st IEEE Conference on Decision and Control (CDC)*, pp. 3551–3556, Maui, HI, USA, December 2012.

[15] A. Hladio, C. Nielsen, and D. Wang, "Path following for a class of mechanical systems," *IEEE Transactions on Control Systems Technology*, vol. 21, no. 6, pp. 2380–2390, 2013.

[16] G. M. Dovgobrod, "Generation of a highly-smooth desired path for transverse feedback linearization," *Gyroscopy and Navigation*, vol. 8, no. 1, pp. 63–67, 2017.

[17] V. T. Nguyen, C. Sentouh, P. Pudlo, and J. Popieul, "Path following controller for electric power wheelchair using model predictive control and transverse feedback linearization," in *Proceedings of the 2018 IEEE International Conference on Systems, Man, and Cybernetics (SMC)*, pp. 4319–4325, Toronto, ON, Canada, March 2018.

[18] Y. Li and C. Nielsen, "Synchronized closed path following for a differential drive and manipulator robot," *IEEE Transactions on Control Systems Technology*, vol. 25, no. 2, pp. 704–711, 2016.